ACS OMEGA

Open Access

http://pubs.acs.org/journal/acsodf

Article

Adjusting the Dose of Ag-Ion Implantation on TiN−Ag-Modified SLA-Ti Creates Different Micronanostructures: Implications on Bacteriostasis, Biocompatibility, and Osteogenesis in Dental Implants

Ming Ma,[#] Mengli Zhao,[#] Ruotong Ji, Yi Guo, Dejun Li,[*] and Sujuan Zeng[*]

Cite This: *ACS Omega* 2023, 8, 39269−39278

Read Online

ACCESS | Metrics & More | Article Recommendations | Supporting Information

ABSTRACT: The prevention of aseptic loosening and peri-implantitis is crucial for the success of dental implant surgery. In this study, different doses of Ag-implanted TiN/Ag nanomultilayers were prepared on the sandblasting with large grit and acid etching (SLA)-Ti surface using a multiarc ion-plating system and an ion-implantation system, respectively. The physical and chemical properties of the samples were assessed using various techniques, including scanning electron microscopy, energy-dispersive spectroscopy, X-ray diffraction, X-ray photoelectron spectroscopy, atomic force microscopy, inductively coupled plasma atomic emission spectrometry, and water contact angle measurements. In addition, the applicability and biosafety of the SLA/1 × 10^{17}-Ag and SLA/1 × 10^{18}-Ag surfaces were determined via biocompatibility testing in vivo and in vitro. The results demonstrated that the physical and chemical properties of SLA/1 × 10^{17}-Ag and SLA/1 × 10^{18}-Ag surfaces were different to some extent. However, compared with SLA-Ti, silver-loaded TiN/Ag-modified SLA-Ti surfaces (SLA/1 × 10^{18}-Ag) with enhanced bacteriostatis, osteogenesis, and biocompatibility have great potential for dental applications.

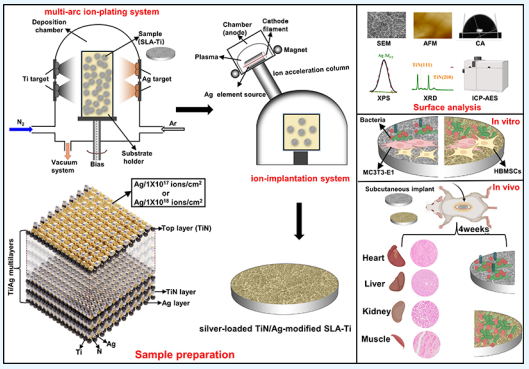

1. INTRODUCTION

Microrough titanium surfaces formed by sandblasting with large grit and acid etching (SLA) are currently among the most commonly used surfaces for dental implants.[1,2] Clinical studies have reported that rough titanium implants can significantly improve the osseointegration rate compared with smooth titanium implants.[3] However, the increased surface roughness that promotes cell adhesion also adheres to bacteria,[4] leading to the accumulation of various bacteria that form biofilms on implant surfaces, which are generally considered to be a major predisposing factor for peri-implant infections.[5,6] Peri-implantitis is an inflammatory and destructive disease caused by the abnormal proliferation of different microbial flora around dental implants and has become the most serious complication that can lead to implant failure.[7−9] In addition, aseptic loosening has become a major cause of the failure of titanium-based implants. This condition is characterized by chronic inflammation resulting from the activation of immune cells that come into contact with implant wear debris. Over time, this inflammation can lead to early bone loss and poor integration of the implant, ultimately resulting in the implant loosening and failure.[10−12] To date, there is no effective strategy that can significantly improve the bacteriostatic ability and promote the early osseointegration of titanium implants. Hence, the development of multifunctional surfaces with osteogenic and antibacterial properties for dental implants is an urgent requirement.[13]

In this study, TiN/Ag multilayers were synthesized on micro/nanotitanium surfaces using a multiarc ion-plating system (SA-6T, China). TiN is commonly selected as the top layer because of its exceptional hardness, wear resistance, corrosion resistance, and favorable biocompatibility.[14−17] However, it should be noted that TiN may not possess sufficient antibacterial properties. To ensure the baseline antibacterial properties of the top layer, it was necessary to implant an appropriate dose of Ag ions on the surface of the TiN/Ag multilayer film. Silver-based biomaterials, particularly silver nanoparticles, have broad-spectrum and highly efficient antibacterial properties.[18−21] Further, the possibility of inducing antimicrobial resistance is extremely low.[22,23] In addition, Ag can destroy the cell membrane, cell wall, and

Received: July 4, 2023
Accepted: September 25, 2023
Published: October 12, 2023

https://doi.org/10.1021/acsomega.3c04769
ACS Omega 2023, 8, 39269−39278

outer membrane of bacterial cells, inhibit protein synthesis, and cause bacterial death.[24−26]

Previous studies have revealed that silver-loaded TiN/Ag-modified titanium alloy surfaces possess efficient physicochemical and mechanical properties and biocompatibility and can enhance the osteogenic activity of rat bone mesenchymal stem cells (rBMSCs) in vitro.[15,27] The above research results are based on the deposition of TiN/Ag multilayers on smooth titanium alloy substrates. The titanium surface with a micro/nanostructure formed via large-grain acid-etched sandblasting is the most commonly used surface of dental implants.[28,29] TiN/Ag multilayers are deposited on this microrough surface, and different doses of Ag ions are implanted onto the top layer to form functional interfaces with different morphologies. The mechanism through which these newly formed Ag-loaded interfaces affect the biological behavior of oral bacteria and human bone marrow-derived mesenchymal stem cells (HBMSCs) remains unclear. Studies have revealed that changes in surface morphology not only affect the physical and chemical properties of materials but also significantly affect the biological behavior of cells and bacteria.[30,31] Based on these findings, we combined TiN/Ag multilayers with micro/nanotopography to laminate multilayers on the surface of SLA titanium and implanted doses of 5×10^{16}, 1×10^{17}, 5×10^{17}, and 1×10^{18} ions/cm^2 silver ions onto the top layer. We characterized the physical and chemical properties of four groups of silver-loaded titanium (Supporting Information) and selected two of them (SLA/1×10^{17}-Ag and SLA/1×10^{18}-Ag) for more in-depth biological performance research. The focus was on the biocompatibility of silver-loaded titanium and its impact on inhibiting bacteria associated with peri-implantitis as well as its effect on the osteogenic differentiation of HBMSCs. This is a continuation of our previous work but is quite different from it. Our goal is to prepare silver-loaded TiN/Ag-modified SLA-Ti surfaces with good physicochemical, mechanical, and antibacterial properties as well as the ability to promote osteogenic differentiation for better application in dental implants.

2. MATERIAL AND METHODS

2.1. Sample Preparation. Commercially pure SLA-Ti disks (10 mm in diameter, 1 mm in thickness, WEGO, China) of grade IV were ultrasonically cleaned in ethanol, acetone, and deionized water for 20 min and air-dried. A detailed description of the multilayer deposition and ion implantation processes can be found in our previous work. Briefly, TiN/Ag multilayer structures were fabricated by an arc ion-plating system (SA-6T, China) on the SLA surface. To obtain desirable antimicrobial properties, two doses of Ag ions were implanted on the surface of the multilayer via an ion implantation system (MEVVA80III-100, China). Various SLA-Ti surfaces were examined: SLA-Ti surface, 1×10^{17} ions/cm^2 Ag-implanted TiN/Ag multilayers (SLA/1×10^{17}-Ag), the interface formed by the implantation of 1×10^{17} ions/cm^2 Ag into TiN/Ag multilayers (SLA/1×10^{17}-Ag), and the interface formed by the implantation of 1×10^{18} ions/cm^2 Ag into TiN/Ag multilayers (SLA/1×10^{18}-Ag). Figure 1 displays the flowchart of experiments.

2.2. Surface Characterization. The micro/nanostructured surface morphology and surface element distribution of the titanium samples before and after multilayer deposition and ion implantation were observed by field emission scanning electron microscopy (SEM, SU-8010, Hitachi, Japan) and energy-dispersive spectroscopy (EDS, Bruker, Germany); the surface topography and the roughness of all the samples were measured by atomic force microscopy (AFM) in the tapping mode (MultiMode 8, Bruker, Germany). X-ray photoelectron spectroscopy (XPS, PHI5000 Versaprobe) was used to investigate the chemical composition of all of the samples. The phase composition of the surface of silver-loaded TiN/Ag-modified titanium was characterized by using X-ray diffraction (XRD, D8A, Bruker, Germany) with Cu Kα (40 kV, 20 mA, λ = 1.54056 Å) radiation.

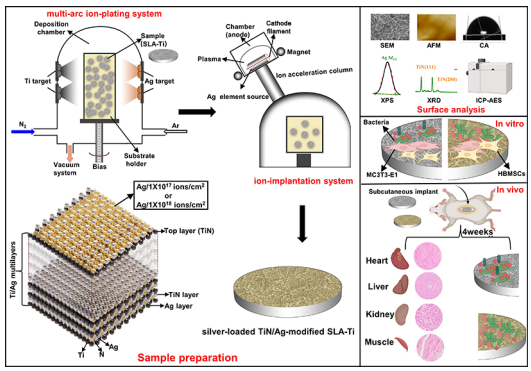

Figure 1. Flowchart of experiments. This diagram was created with BioRender.com.

2.3. Water Contact Angles and Release of Silver. The water contact angles of various SLA-Ti samples were measured by using a contact angle instrument (CAMKSV021733, Finland). The silver-loaded TiN/Ag-modified titanium samples were soaked in 5 mL of Phosphate B uffered Saline (PBS, Gibco, US, PH 7.2) 37 °C for 30 days without stirring. The amounts of released Ag ions were then evaluated by inductively coupled plasma atomic emission spectrometry (ICP-AES; Horiba Jobin Yvon Ultima, Horiba, Japan).

2.4. In Vitro Cytocompatibility Evaluation. *2.4.1. Cell Cultures.* MC3T3-E1 cells (purchased from the Cell Bank of the Chinese Academy of Sciences, Shanghai, China) were used to evaluate the cytocompatibility of various samples. A detailed description of the culture process of MC3T3-E1 cells was presented in our previous study.

2.4.2. Cell Morphology and Cytoskeletal Observations. To observe the cell morphology on various samples, the MC3T3-E1 cells were seeded on the different samples at a cell density of 2.0×10^4 cells/mL. After incubation for 24 h on the samples, the cells were rinsed three times with PBS, followed by fixing with 2.5% glutaraldehyde for 10 h at 4 °C in the dark. Then, they were dehydrated with a graded ethanol series of 30, 50, 75, 90, and 100% ethanol and freeze-dried, and the samples coated with platinum sputtering were then observed using SEM. To observe the cytoskeletal actin, cells were seeded on different SLA-Ti samples at a density of 1×10^4 cells/mL, cultivated for 72 h, immersed in PBS three times and fixed in 4% paraformaldehyde (Sigma, USA) for 20 min on ice, and rinsed thrice with PBS. Afterward, MC3T3-E1 cells attached to the materials were permeabilized with 0.25% Triton X-100 (Amresco, USA) for 10 min at room temperature and washed three times with PBS buffer. The cytoskeletal actin and nucleus of MC3T3-E1 cells were stained with TRITC-Phalloidin (Yeasen, China) and 4,6-diamidino-2-phenylindole (DAPI, Sigma-AldloadedCo, USA) and examined using a fluorescence microscope (Olympus Corporation, Japan).

https://doi.org/10.1021/acsomega.3c04769
ACS Omega 2023, 8, 39269−39278

2.4.3. Cell Proliferation Assay. The cell proliferation on various SLA-Ti disks was measured using a cell counting kit-8 (CCK-8; Dojindo, Japan). Initially, 5.0×10^3 cells/mL was seeded onto all the samples in 24 well plates and cultured for 1, 4, and 7 days. At each time point, the cell culture medium was replaced with 600 μL of CCK-8 reagent solution (diluted with fresh full medium) per well for 3 h at 37 °C, away from light. Then, 100 μL of the supernatant was transferred to a black 96 well plate to examine the optical density (OD) at 450 nm using a plate reader (BIO TEK, ELX 800).

2.4.4. Live/Dead Assay. The cytotoxicity of silver-loaded TiN/Ag-modified titanium samples on MC3T3-E1 cells was measured by the live/dead staining kit (Abcam, USA) strictly following the manufacturer's instructions. Briefly, MC3T3-E1 cells (2.0×10^4 cells/mL) were seeded on various SLA-Ti surfaces and cultured for 3 days. All of the samples were then transferred to a new 24 well plate and washed with PBS buffer thrice. MC3T3-E1 cells on the samples were stained with green fluorescence (live cells) after reacting with 2.5 μM calcein-AM and red fluorescence (dead cells) after reacting with 5 μM PI for 20 min at room temperature, away from light. Representative images were obtained by a confocal laser scanning microscope (CLSM, Olympus).

2.5. Osteogenic Activity In Vitro. *2.5.1. Cell Cultures.* Human bone marrow stromal cells (HBMSCs, ATCC, Manassas, VA, USA) were cultured in a humidified incubator at 37 °C, 5% CO_2 where α-minimum essential medium (α-MEM, containing 1% antibiotic/antimycotic solution and 10% fetal bovine serum) was changed every 2−3 days, and only HBMSCs of passages 2−6 were used in the experiments.

2.5.2. Alkaline Phosphatase Staining Assay. HBMSCs (7×10^4 cells/mL) were seeded on various samples in triplicate into 24 well plates after 7 and 14 days of cultivation for alkaline phosphatase (ALP) staining. Then, ALP staining was performed using the BCIP/NBT (5-Bromo-4-chloro-3-indolyl phosphate/etranitroblue tetrazolium chloride) ALP kit (Beyotime, Biotechnology, China) according to the manufacturer's instructions. Images of stained samples were taken using a stereomicroscope (Olympus, Japan).

2.5.3. Immunofluorescence Staining. HBMSCs were seeded on different SLA-Ti surfaces at a density of 5×10^4 cells/well for 7 days in osteogenic induction DMEM medium (Dulbecco's modified Eagle's medium) containing dexamethasone (10 mM, 1 μL), ascorbic acid (5 mg/mL, 1 mL), and β-sodiumglycerophosphate (1 M, 1 mL) per 100 mL. The immunofluorescence staining procedure was described in a previous report.[32] In brief, at day 7, HBMSCs adhered to the samples were fixed with paraformaldehyde (4%) for 20 min and permeabilized by 0.25% Triton X-100 for 15 min, followed by blocking with 5% bovine serum albumin (BSA) solution (Sigma-Aldloaded) for 1 h at room temperature. Then, HBMSCs on the surfaces were treated with anti-ALP (1:200, Abcam) and antirunt-related transcription factor 2 (RUNX2, 1:350, Santa Cruz) primary antibodies overnight at 4 °C to detect the levels of ALP and RUNX2. All of the samples were incubated and counterstained with secondary antibodies (DyLight 488-conjugated IgG and DyLight 549 IgG antibodies, CST, USA) and 4,6-diamidino-2-phenylindole dihydrochloride (DAPI, Sigma, USA). Finally, the stained cells were observed by a CLSM imaging system, and the relative fluorescence intensity was quantified by using ImageJ software (ImageJ, Wayne Rasband).

2.6. In Vitro Antibacterial Ability. The antibacterial effects of silver-loaded TiN/Ag-modified titanium surfaces were measured by using Gram-negative *Fusobacterium nucleatum* (ATCC 25586) and *Staphylococcus aureus* (ATCC 25923). *F. nucleatum* was cultured in brain heart infusion supplemented with additional ingredients (1% heme and 1% menadione in Brian Heart Infusion solution, 37 °C), followed by anaerobic incubation for 24 h, whereas *S. aureus* was cultured in brain heart infusion broth medium at 37 °C under aerobic conditions.

All sterilized titanium samples were inoculated with *F. nucleatum* and *S. aureus* bacterial suspension (100 μL, 1×10^7 CFU/mL) at 37 °C in anaerobic and aerobic environments, respectively. After 24 h of incubation, all samples were rinsed thrice with PBS solution to remove unattached bacteria, while adhered bacteria were detached from the samples via an ultrasonic cleaner (150 W, 50 Hz, 10 min) and a shaker (maximum power, 5 min). The isolated bacteria were serially diluted on agar plates (*S. aureus*) or sheep blood agar plates (*F. nucleatum*) and recultivated for 24 (*S. aureus*) and 48 h (*F. nucleatum*) in triplicate, respectively. The number of active bacteria was counted according to the National Standard of China GB/T 4789.2 protocol, and the antibacterial rates (Ra) of SLA-Ti, SLA/1 × 10^{17}-Ag and SLA/1 × 10^{18}-Ag were calculated as follows: Ra (%) = (A − B) /A × 100%, where A is the average number of *S. aureus* and *F. nucleatum* on the SLA-Ti group, and B is the average number of *S. aureus* and *F. nucleatum* on the SLA/1 × 10^{17}-Ag or SLA/1 × 10^{18}-Ag group.

2.7. Histocompatibility and Antibacterial Stability in Mice. Animal experiments were conducted according to Chinese animal welfare guidelines and experimental protocols. All experiments were approved by the Animal Ethics Committee of Guangdong Huawei Testing Co. Ltd. (NO:202210003; HWT-BG-117). Silver-loaded TiN/Ag-modified Ti samples and SLA-Ti (control) were subcutaneously implanted into ICR (Institute of Cancer Research) mice to evaluate their in vivo biosafety and in vitro antimicrobial stability. ICR mice of 6−8 weeks of age were used in this study (N = 3 mice per group). Subcutaneous implantation surgeries were performed according to the established protocols. Briefly, a 1 cm skin incision was made at the midline of the back and subcutaneous pocket, and various SLA-Ti samples (Ø10 × 1 mm, one disk per mouse) were implanted. Four weeks after subcutaneous implantation, mice were sacrificed by carbon dioxide asphyxiation, and the tissues surrounding the implanted samples and important organs were removed. The obtained samples were fixed in 10% neutral formalin overnight, embedded in paraffin, and sectioned (3 μm) for hematoxylin and eosin (H&E) staining to examine the histocompatibility of silver-loaded titanium samples. The bacteriostatic effect of the SLA-Ti samples obtained from the animals was measured via live/dead cell staining, as previously described.[32]

2.8. Statistical Analysis. The GraphPad Prism 7 (La Jolla, CA, USA) software was used for the statistical analyses, and all data were reported as means ± standard deviation (SD). Significance levels were determined using one-way ANOVA combined with the Student−Newman−Keuls post hoc test, and $p < 0.05$ and $p < 0.01$ are statistically and highly significant, respectively.

https://doi.org/10.1021/acsomega.3c04769
ACS Omega 2023, 8, 39269−39278

3. RESULTS AND DISCUSSION

3.1. Surface Characterization. The SEM results reveal that the SLA-Ti- and TiN/Ag-modified SLA-Ti surfaces display honeycomb multilevel micro- and nanostructures (Figure 2A). The surface morphology of the material is

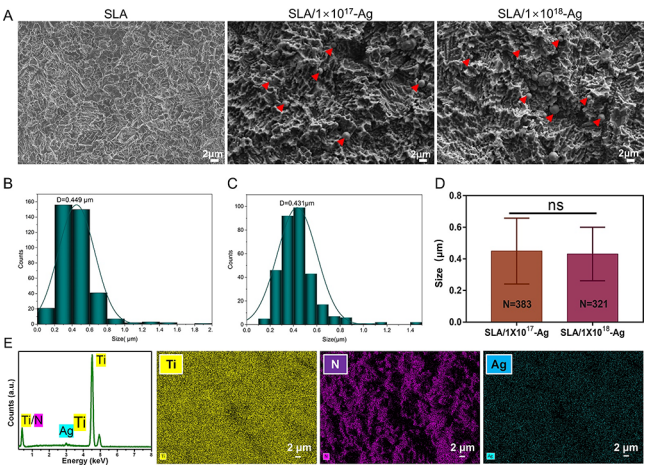

Figure 2. Surface morphology of SLA-Ti surface after TiN/Ag modification examined by SEM: (A) SLA-Ti, SLA/1 × 10^{17}-Ag, SLA/1 × 10^{18}-Ag; size distributions of the particles on (B) SLA/1 × 10^{17}-Ag, (C) SLA/1 × 10^{18}-Ag, (D) comparison of particle size on SLA/1 × 10^{17}-Ag, SLA/1 × 10^{18}-Ag surfaces, and (E) EDS analyses of SLA/1 × 10^{18}-Ag.

significantly altered with the TiN/Ag film coated in the top layer when compared to SLA titanium. However, no obvious microstructural evolution can be observed on the control titanium surface after TiN/Ag modification and implantation of silver ions at different doses. The red arrows indicate particles that may be Ag agglomerated, and all nanosilver particles are evenly distributed on the SLA titanium surfaces. For SLA/1 × 10^{17}-Ag, the average diameter of the silver nanoparticles is approximately 449 nm (Figure 2B), which decreases to 431 nm when the silver ion implantation dose is increased to 1 × 10^{18} ions/cm^2 (Figure 2C). There is no significant difference in the average diameter of the silver nanoparticles between the silver-loaded TiN/Ag-modified SLA-Ti surfaces ($p > 0.05$).

Figure 3A shows the three-dimensional images and roughness of the silver-loaded TiN/Ag-modified SLA-Ti surfaces that were drawn based on AFM, including the arithmetic mean

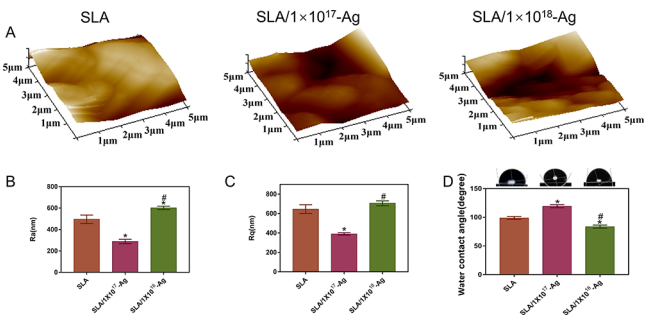

Figure 3. 3D images of surface topography, roughness, and water contact angle of different samples. (A) 3D images of surface topography, (B) Ra roughness, (C) Rq roughness, and (D) water contact angles (*$p < 0.05$, **$p < 0.01$, ***$p < 0.001$).

of the surface roughness (R_a) and root-mean-square of the surface roughness (R_q) of TiN-Ag-modified SLA-Ti with different doses of silver ions. Compared to the top layer without Ag-ion implantation, the surface roughness of the top layer implanted with Ag ions first decreases and then increases with a change in the implantation dose of Ag ions. Specifically, the roughness parameters are minimal (R_a = 285 nm and R_q = 393 nm) when the TiN/Ag multilayer is implanted at an Ag-ion dose of 1 × 10^{17} ions/cm^2. However, when the implantation dose of the Ag ions is increased to 1 × 10^{18} ions/cm^2, the roughness reaches its maximum value (R_a = 595 nm, R_q = 570 nm). The roughness parameters of the SLA-Ti surface are between those of the Ag-loaded TiN/Ag-modified samples. These results are shown in Figure 3B,C. The surface of the SLA/1 × 10^{17}-Ag group sample is flatter than that of SLA titanium, which may be because the honeycomb structure and multilevel pores on the SLA titanium surface are filled with the formation of a TiN/Ag multilayer and the implantation of silver ions. As the dose increases, more high-energy ions bombard the samples, causing more nanosilver particles to get deposited on the SLA titanium, which destroys the compactness and flatness of the multilayer film surface. The above results reveal that within a certain range, the dose of silver ion implantation has an impact on the surface morphology of the material. The EDS results (Figure S1) show the SLA-Ti surface contains Ti (atomic percent of 76.26%), O (19.79%), and C (3.95%). Therein, the content of Ti is the main component, where a small amount of O comes from the oxidation of Ti on the surface. The trace C may come from the impurities adsorbed on the surface of the SLA. For SLA/1 × 10^{17}-Ag (Figure S1) and SLA/1 × 10^{18}-Ag (Figure 2E), in addition to Ti, their surfaces also contain evenly distributed N and Ag, confirming that the surface of SLA-Ti may contain Ag and TiN.

Figure 3D displays the wettability of the sample surface. The water contact angle of the SLA-Ti sample is approximately 98.8 ± 2.01° and increases to 119.3 ± 2.15° for the SLA/1 × 10^{17}-Ag group sample, whereas it decreases to 83.7 ± 2.23° for the SLA/1 × 10^{18}-Ag group. This indicates that SLA/1 × 10^{18}-Ag surfaces are more hydrophilic than SLA/1 × 10^{17}-Ag and SLA-Ti surfaces. According to the AFM and SEM results, the surface roughness of the silver-loaded titanium first decreases and then increases with an increase in the silver ion implantation dose. Studies have revealed that there is a positive correlation between the surface roughness and wettability of materials; that is, within a certain range, an increase in the surface roughness improves the wettability.[33,34] In summary, the changes in the roughness and wettability of the surfaces of each group of materials are consistent with the previously reported results. The SLA/1 × 10^{18}-Ag surface has the highest surface roughness among the three groups of materials and is, therefore, the most hydrophilic.

The SLA/1 × 10^{17}-Ag and SLA/1 × 10^{18}-Ag samples were immersed in PBS for 30 days for ICP-AES. The values obtained from the SLA/1 × 10^{17}-Ag and SLA/1 × 10^{18}-Ag groups are both less than 5 ppb, indicating that the Ag ions are effectively fixed on the top layer and that trace amounts of Ag leach from the SLA/1 × 10^{17}-Ag and SLA/1 × 10^{18}-Ag samples. Table 1 describes the release of the silver ions.

Figure 4 shows the XRD patterns of the various surfaces. According to standard card PDF#44−1294, SLA is hexagonal titanium. The SLA/1 × 10^{17}-Ag and SLA/1 × 10^{18}-Ag surfaces show TiN (111) and TiN (200) orientations, indicating that

https://doi.org/10.1021/acsomega.3c04769
ACS Omega 2023, 8, 39269−39278

Table 1. Silver Ion Concentration in PBS Solution after Immersion for 30 days

immersion time (days)	30
SLA (μg/mL)	0
SLA/1 × 10^{17}-Ag (μg/mL)	<0.005
SLA/1 × 10^{18}-Ag (μg/mL)	<0.005

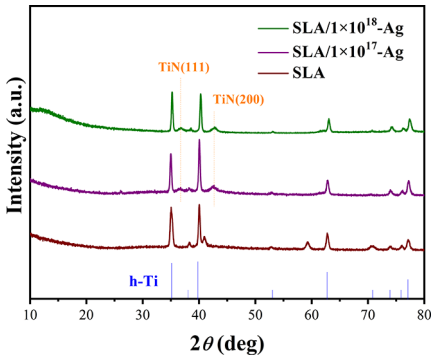

Figure 4. X-ray diffraction patterns of TiN/Ag multilayers at different Ag^+ doses.

TiN grains form on the surfaces. The content of silver prepared by ion implantation is very low, and the thickness of the Top TiN film is thick (according to the deposition rate, the thickness of top TiN is ~300 nm), resulting in the associated peaks not being detected using the XRD. To further determine whether silver is successfully implanted on the top layers, the chemical states and elemental composition of all samples were analyzed using XPS. The results show that Ti and N are present in all the samples. In addition, Ag peaks are found in SLA/1 × 10^{17}-Ag and SLA/1 × 10^{18}-Ag, indicating successful Ag implantation (Figure 5A). Moreover, the atomic percentages of Ag in SLA/1 × 10^{17}-Ag and SLA/1 × 10^{18}-Ag are 0.16 and 0.27%, respectively. Further analysis was conducted using a high-resolution Ag3*d* spectrum, as shown in Figure 5B. The results indicate that metallic silver is present on the surfaces of silver-loaded TiN/Ag-modified SLA-Ti in the form of Ag3*d*3/2 and Ag3*d*5/2, located at approximately 374.4 and 368.4 eV, respectively.[35]

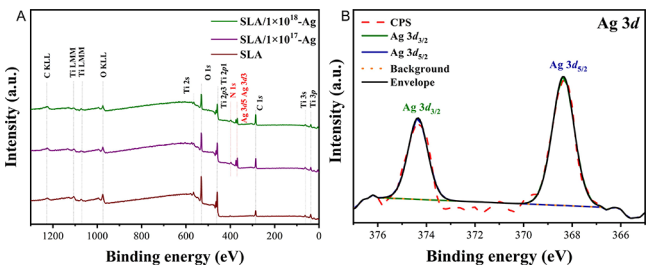

Figure 5. (A) XPS survey spectrum of three sample groups. (B) High-resolution Ag 3d XPS spectra of different samples.

3.2. In Vitro Bacteriostasis Assays and Possible Antibacterial Mechanisms. Implant surfaces with broad-spectrum antibacterial properties are critical for the clinical application of oral implants because the most commonly used dental implants in clinical practice do not have bacteriostatic properties. During the early stages of implantation, the surfaces of the implant and surrounding tissues are often invaded by various bacteria.[32,36] If not treated in a timely manner, peri-implantitis is likely and can eventually lead to failure of the implant surgery. Bacterial infections on implant surfaces are characterized by the formation of biofilms that protect bacterial colonies on the material surface,[32] contributing to bacterial persistence. In this study, Gram-positive *S. aureus*, which is associated with the formation of dental plaque biofilms, and Gram-negative bacteria *Porphyromonas gingivalis*, which is closely related to the development of peri-implantitis, were selected to evaluate the in vitro inhibitory effect of silver-loaded titanium.

The bacteria that were cultured and adhered to the surface of all samples for 24 h were isolated and recultured on the corresponding agar plates based on plate counting methods. In addition, Ra relative to SLA-Ti was used to quantitatively evaluate the antimicrobial properties of the silver-loaded TiN/Ag-modified SLA-Ti surfaces. As shown in Figure 6A, a large number of viable bacteria were detected and cultured on the SLA-Ti surface, and a large number of bacteria detached from the surface, indicating that the two doses of silver-loaded TiN/Ag-modified SLA-Ti surfaces have stronger inhibitory effects on peri-implantitis-related bacteria. The antibacterial ability of the SLA/1 × 10^{18}-Ag surface is superior to that of the SLA/1 × 10^{17}-Ag surface, regardless of whether it is *F. nucleatum* or *S. aureus*, indicating that the silver ion implantation dose positively correlates with the antibacterial effect. Notably, the antibacterial activity of the silver-loaded TiN/Ag-modified SLA-Ti surfaces on *S. aureus* is lower than that on *F. nucleatum*. Specifically, the rates of the antibacterial activity of SLA/1 × 10^{17}-Ag surface on *S. aureus* and *F. nucleatum* are 81.39 and 88.17%, respectively (Figure 6B,C), and the rates of the antibacterial activity of SLA/1 × 10^{18}-Ag surface on *S. aureus* and *F. nucleatum* are 90.63 and 94.81%, respectively (Figure

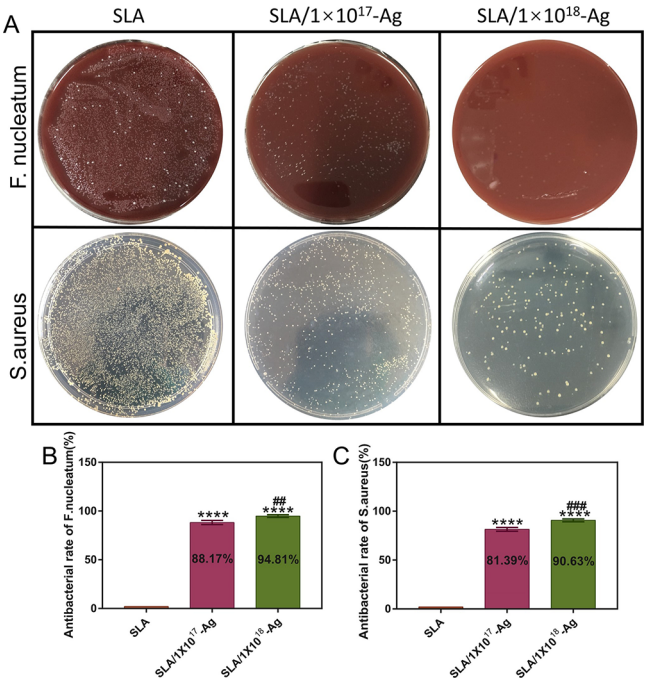

Figure 6. Antibacterial effects of *F. nucleatum* and *S. aureus* on various samples after 24 h. (A) Colony images of *F. nucleatum* and *S. aureus* by the spread plate method, (B) antibacterial rates of *F. nucleatum* on different samples, and (C) antibacterial rates of *S. aureus* on various samples (*p < 0.05, **p < 0.01, ***p < 0.001).

https://doi.org/10.1021/acsomega.3c04769
ACS Omega 2023, 8, 39269−39278

6B,C). Therefore, *F. nucleatum* is more susceptible to Ag-NPs than *S. aureus*, which may be due to the difference in the structure and composition of the cell wall between Gram-negative and Gram-positive strains.

Antibacterial mechanisms of nanosilver particles have been reported in several studies; however, they remain controversial. The following three antibacterial mechanisms of nanosilver particles are widely accepted: (1) nanosilver particles directly damage the outer membrane, cell wall, and cell membrane of bacteria, changing the permeability of the cell membrane and finally causing cell leakage.[37,38] (2) The presence of Ag ions and Ag particles in bacterial cells leads to the production of reactive oxygen species (ROS), which cause oxidative stress and ultimately apoptosis.[39] (3) Silver ions can bind to thiol groups on bacterial proteins, resulting in DNA degradation and metabolic dysfunctions, such as respiratory reactions, lipid synthesis, and protein synthesis impairment.[40] Based on the above antibacterial mechanisms and the results of silver ion release in the solution, it can be deduced that silver ion sterilization is not the key antibacterial mechanism of silver-loaded TiN/Ag-modified SLA-Ti surfaces, and that neutral metallic silver (Ag0) on the SLA/1 × 10^{17}-Ag and SLA/1 × 10^{18}-Ag surfaces play a dominant role in exerting the antibacterial effect. The underlying factors leading to the antibacterial effects of Ag-NPs are similar to those reported by Zhao et al.,[17] Cao and co-workers,[40] and Zhu et al.[41] Figure 7 shows the possible antibacterial mechanism of the silver-loaded TiN/Ag-modified SLA-Ti surfaces.

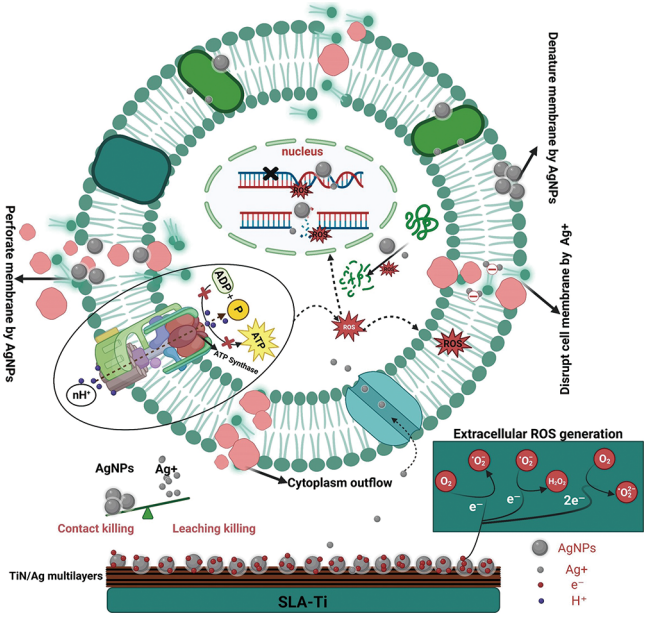

Figure 7. Illustration of the possible bacteriostatic mechanism on silver-loaded TiN/Ag-modified SLA-Ti. This diagram was created with BioRender.com.

3.3. Cytocompatibility Evaluation. To investigate the interaction between the MC3T3-E1 cells and the samples, the morphology and cytoskeleton (F-actin) of the MC3T3-E1 cells grown on various surfaces were observed by using SEM (day 1) and CLSM (day 3). As shown in Figure 8A, after culturing for 24 h, the MC3T3-E1 cells on the surface of all materials were polygonal and spread well, and a large number of pseudopodia were fixed on the surface of the material. On day

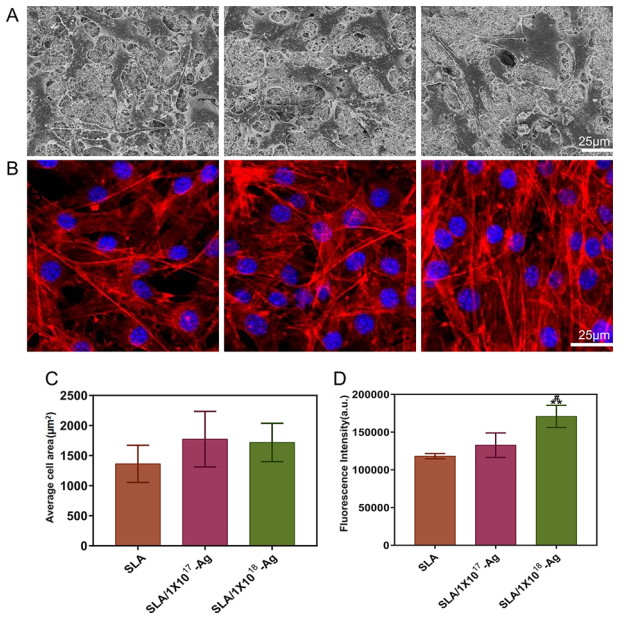

Figure 8. (A) SEM images of MC3T3-E1 cells on various samples for 1 day, (B) fluorescent images of MC3T3-E1 cells cultured on various surfaces for 3 days with actin stained with TRITC-Phalloidin (red) and nuclei stained with DAPI (blue), (C) average areas of MC3T3-E1 cells adhering to three groups of samples, and (D) quantitative analysis data of fluorescence intensity (*, #$p < 0.05$ compared with SLA-Ti and SLA/1 × 10^{17}-Ag, respectively, **$p < 0.01$, ***$p < 0.001$).

1, ImageJ software was used to quantitatively analyze the distribution of cell adhesion on the surfaces of all materials. The results reveal that the average area of the MC3T3-E1 cells adhered to the silver-loaded TiN/Ag-modified SLA-Ti surface is not significantly different from that of SLA-Ti (Figure 8C). However, after 3 days of incubation (Figure 8B), the MC3T3-E1 cells adhered to all samples, rapidly proliferated, and completely covered the titanium surface (CLSM). Compared with cells attached to the SLA-Ti surface, those on the silver-loaded TiN/Ag-modified SLA-Ti surfaces display greater F-actin expression and more filopodia and lamellipodia, and the cells are connected by filopodia, which is conducive to cell proliferation (Figure 8B). To gain a deeper understanding of the behavior of MC3T3-E1 cells on various samples, we quantified the expression of the F-actin protein in cells adhered to the surface of each group of materials, revealing significant differences ($p < 0.05$) in the fluorescence intensity among SLA-Ti, SLA/1 × 10^{17}-Ag, and SLA/1 × 10^{18}-Ag (Figure 8D). Further, there is no significant difference in the expression of F-actin protein in the cells that adhered to the surfaces of SLA/1 × 10^{17}-Ag and SLA-Ti, indicating that the SLA/1 × 10^{17}-Ag surface does not affect the spreading and initial adhesion of MC3T3-E1 cells. Interestingly, the SLA/1 × 10^{18}-Ag surface is the main interface promoting the expression of F-actin in the MC3T3-E1 cells among the three groups, and the expression level of F-actin is significantly different from that in the other two groups (SLA-Ti and SLA/1 × 10^{17}-Ag). This suggests that controlling the implanted dose of silver within a certain range can lead to an increase in the expression of the F-actin protein and better adhesive properties in MC3T3-E1 cells as the dose of silver ion implantation increases.

The viability and proliferation of MC3T3-E1 cells on various samples were evaluated qualitatively using a live/dead

https://doi.org/10.1021/acsomega.3c04769
ACS Omega 2023, 8, 39269−39278

viability/cytotoxicity kit (Abcam, USA) and quantitatively using the CCK-8 detection kit (Dojindo, Japan) after culturing for 1, 4, and 7 days. Generally, calcein-AM enters living cells and fluoresces green, whereas PI enters dead cells and fluoresces red. As shown in Figure 9A–C, calcein-AM/PI

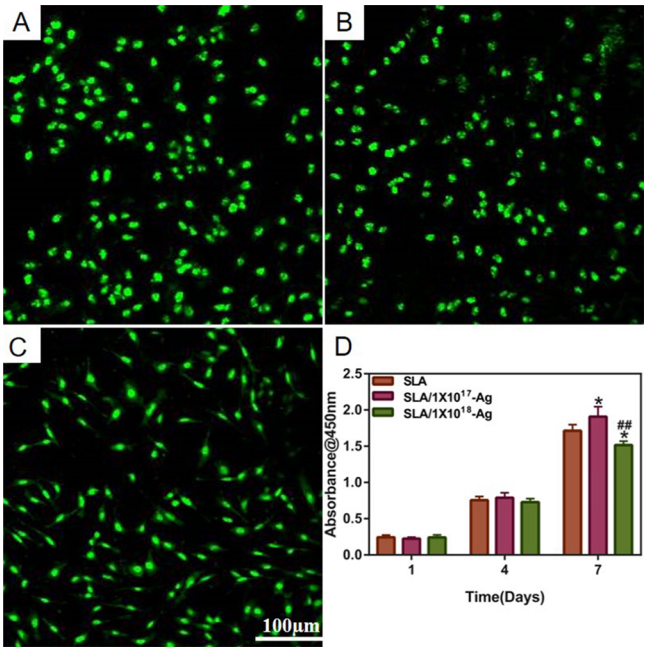

Figure 9. Viability of MC3T3-E1cells cultured for 3 days on various SLA-Ti surfaces labeled by calcein-AM (live cells, green); PI staining (dead cells, red). (A) SLA, (B) SLA/1 × 10^{17}-Ag, and (C) SLA/1 × 10^{18}-Ag. The proliferation of MC3T3-E1 cells cultured on different SLA-Ti surfaces at different times (D). *, #: $p < 0.05$ compared with -Ti and SLA/1 × 10^{17}-Ag, respectively.

staining reveals that MC3T3-E1 cells have favorable growth on various titanium samples, and only live cells (green staining) and a small number of dead cells (red staining) are observed in all of the samples after 3 days of incubation, suggesting that both SLA-Ti and silver-loaded TiN/Ag-modified SLA-Ti surfaces have good cytocompatibility with MC3T3-E1cells. The CCK-8 assay results (Figure 9D) reveal that MC3T3-E1 cells on different SLA-Ti samples proliferate over time, and the OD values of the seeded SLA-Ti and silver-loaded TiN/Ag-modified SLA-Ti surfaces increase with time (1, 4, and 7 days). However, the OD values obtained for the SLA/1 × 10^{18}-Ag group are slightly lower than those of the SLA/1 × 10^{17}-Ag and SLA-Ti groups ($p < 0.05$) on day 7 of the culture, indicating that the SLA/1 × 10^{18}-Ag group has a slightly negative impact on the MC3T3-E1 cells. Several researchers have confirmed these results and observed greater cell proliferation on titanium surfaces with decreasing roughness.[42−45] Therefore, the high roughness of the SLA/1 × 10^{18}-Ag surface may be responsible for its slightly lower cell proliferation ability compared to that of the other two groups. Overall, based on the adhesion, proliferation, and viability of MC3T3-E1 cells on silver-loaded TiN/Ag-modified SLA-Ti surfaces, we conclude that silver-loaded titanium surfaces have acceptable cytocompatibility and are promising candidates for dental implant applications.

3.4. Alkaline Phosphate Activity and Osteo-Related Marker Expression. Alkaline phosphatase is a pivotal marker of early osteogenesis. As shown in Figure 10A, HBMSCs

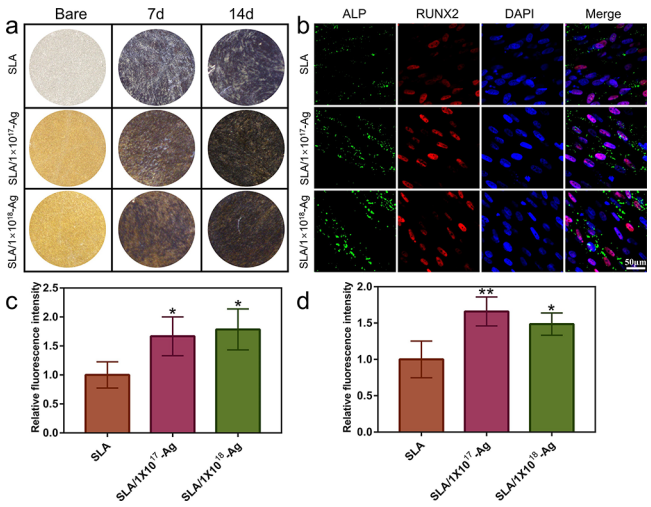

Figure 10. Effect of various SLA-Ti surfaces on osteogenic differentiation of HBMSCs under the osteoinductive condition. (A) Representative staining of ALP on days 7 and 14. (B) Representative immunofluorescent images of typical osteogenic markers (ALP, RUNX2) in HBMSCs cultured on various samples for 7 days. Quantitative analysis data of relative fluorescence intensity of (C) ALP and (D) RUNX2 (*$p < 0.05$, **$p < 0.01$).

cultured on SLA-Ti and silver-loaded TiN/Ag-modified SLA-Ti surfaces for 7 and 14 days were stained using an ALP staining kit. The ALP-positive area in the three groups of samples after 14 days is much stronger than that after 7 days, indicating that the silver-loaded TiN/Ag-modified SLA-Ti surfaces have no adverse effect on the osteogenic differentiation of HBMSCs in terms of ALP production. However, it is difficult to directly compare the differences in ALP-stained-positive areas between SLA-Ti and silver-loaded TiN/Ag-modified SLA-Ti because of the different colors of the substrates. Notably, ALP staining shows larger areas and a darker coloration of HBMSCs on SLA/1 × 10^{18}-Ag than on SLA/1 × 10^{17}-Ag after osteogenic differentiation, indicating that an increase in the dose of silver ion implantation may promote the early osteogenic differentiation of HBMSCs.

ALP and RUNX2 are early markers of osteogenesis. To further investigate the osteogenic differentiation ability of various SLA-Ti surfaces, we assessed the osteogenic differentiation of HBMSCs via ALP and RUNX2 immunofluorescence staining (Figure 10B). On day 7, all osteo-associated proteins (ALP and RUNX2) are upregulated in the silver-loaded TiN/Ag-modified SLA-Ti surfaces compared with the SLA-Ti group ($p < 0.05$). In addition, the expression levels of ALP are slightly higher in the SLA/1 × 10^{18}-Ag group than in the SLA/1 × 10^{17}-Ag group, which is consistent with the ALP staining results (Figure 10C). Simultaneously, the expression levels of RUNX2 in the SLA/1 × 10^{18}-Ag group are slightly lower than those in the SLA/1 × 10^{17}-Ag group (Figure 10D). In summary, the silver-loaded TiN/Ag-modified SLA-Ti surfaces (SLA/1 × 10^{17}-Ag and SLA/1 × 10^{18}-Ag) promote the osteogenic differentiation of HBMSCs. The surface morphology of titanium directly affects the physiological functions of HBMSCs. The surfaces of SLA titanium and silver-loaded TiN/Ag-modified SLA-Ti present a functional interface composed of micro/nanostructures, which can simulate the microenvironment of the body to the greatest extent and strengthen the adsorption of the extracellular matrix. Therefore, we speculate that the combination of

https://doi.org/10.1021/acsomega.3c04769
ACS Omega 2023, 8, 39269−39278

composition and structure is responsible for the better osteogenic activity of the silver-loaded TiN/Ag-modified SLA-Ti surfaces. Overall, silver-loaded TiN/Ag-modified SLA-Ti can promote early osteogenic differentiation of HBMSCs, which may avoid and reduce the occurrence of early aseptic loosening and may be suitable for dental implants. In addition, the osseointegration ability of Ag-loaded titanium must be further verified in animal experiments.

3.5. Histocompatibility and Bacteriostatic Stability in Mice. In vivo biosafety has always been a critical issue in the use of Ag nanomaterials in biomedical applications. When biomaterials are transplanted into the human body, they elicit different responses in the host. The release of Ag ions and nanoparticles from the Ag-loaded TiN/Ag-modified SLA-Ti surface may lead to biological toxicity in the surrounding tissues and vital organs. As shown in Figure 11A, various

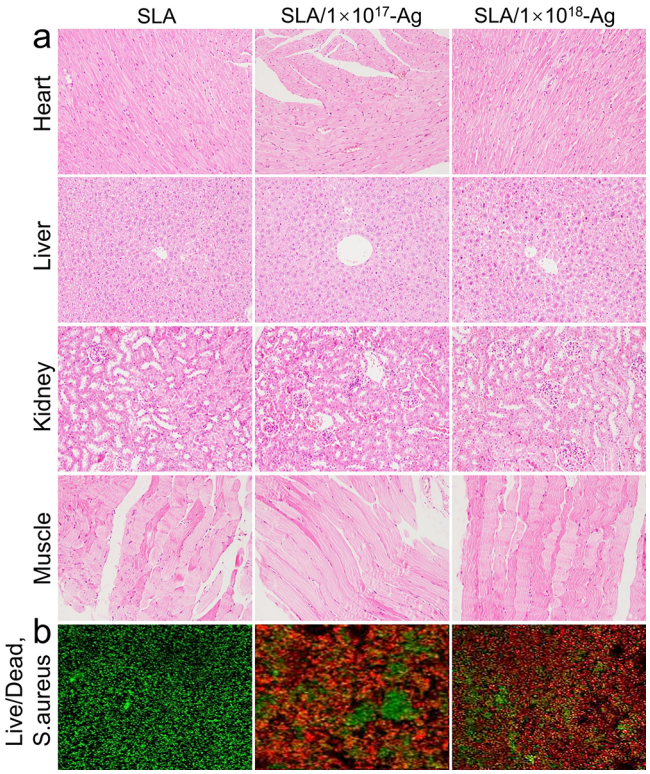

Figure 11. Biosafety analysis in the implantation model (histopathological analysis of surrounding tissues and major organs after subcutaneous implantation in mice) and histological evaluations (A) and in vitro antibacterial (B) magnification: × 200.

samples were implanted into ICR mice (4 weeks old), and the adjacent tissues and major organs (the heart, liver, and kidney) of the ICR mice were observed via H&E staining. The results of H&E staining reveal that there are no pathological changes in the tissues around the implant and important organs of ICR mice, indicating that the TiN/Ag-modified SLA-Ti surface has good biocompatibility in vivo.

When considering clinical applications, it is crucial to consider the bacteriostatic and long-term antibacterial properties of implants within the human body. Peri-implant infection can occur at any time after implantation; however, research indicates that the highest risk of infection occurs within the first 4 weeks. This is because the osseointegration interface has not yet formed, and the body's ability to fight infection is relatively weak during this period.[46,47] To assess the long-term efficacy and stability of the antibacterial properties of Ag-loaded titanium, the samples were subcutaneously implanted into ICR mice for 4 weeks. The collected samples were cleaned and sterilized for in vitro analysis of the antibacterial performance of silver-loaded TiN/Ag-modified SLA-Ti. Recent studies have indicated that *S. aureus* is the main bacterium in the early stages of peri-implant infection.[47] Therefore, we evaluated the bacteriostasis of silver-loaded TiN/Ag-modified SLA-Ti surfaces against *S. aureus* using live and dead staining assays. The live/dead assay is a common method to distinguish live bacteria from dead ones based on the color change; SYTO 9 in the reagent component can stain all live bacteria green, whereas PI only penetrates bacteria with damaged cell membranes and stains the dead bacteria red. As shown in Figure 11B, all samples were immersed in a bacterial suspension (*S. aureus*) for 24 h to test their antibacterial performance. For *S. aureus*, the red spots cover almost the entire SLA-Ti surface, whereas the majority of the green spots are on the SLA/1 × 10^{17}-Ag and SLA/1 × 10^{18}-Ag surfaces, indicating that the antibacterial properties are significantly higher than those on the SLA-Ti surfaces. The above results show that silver-loaded TiN/Ag-modified SLA-Ti surfaces have longevity and stable antibiofilm properties.

4. CONCLUSIONS

In summary, silver-loaded TiN/Ag multilayers were fabricated on an SLA-Ti surface using multiarc ion-plating and ion implantation systems. Two new functional interfaces with different micro/nanostructures (SLA/1 × 10^{17}-Ag and SLA/1 × 10^{18}-Ag surfaces) were formed on the SLA-Ti surface by changing the implantation dose of silver ions on the top layers. Compared with the SLA-Ti and SLA/1 × 10^{17}-Ag groups, the SLA/1 × 10^{18}-Ag surface had the best hydrophilicity, which may be related to its largest surface roughness. The XRD results showed that the preferred orientation of the TiN phase was (111) and that the size of the TiN grains decreased as the Ag^{+} dose increased. Our silver-loaded TiN/Ag-modified SLA-Ti surfaces can not only efficiently inhibit the adhesion and proliferation of bacteria associated with peri-implantitis but also promote the osteogenic differentiation of HBMSCs. In addition, the silver-loaded TiN/Ag-modified SLA-Ti surfaces exhibited good biocompatibility in vitro and in vivo. The combination of composition (silver dose) and structure (micro/nanostructure) may be the critical factor determining the biological performance of silver-loaded TiN/Ag-modified SLA-Ti. Considering the antibacterial properties, osteogenic activity, and biocompatibility of materials comprehensively, we hypothesize that the SLA/1 × 10^{18}-Ag surface may be highly suitable for dental applications and possesses great clinical potential.

■ ASSOCIATED CONTENT

Supporting Information

The Supporting Information is available free of charge at https://pubs.acs.org/doi/10.1021/acsomega.3c04769.

Scanning electron microscopy (SEM) images and energy-dispersive X-ray spectrometry (EDS) mapping images of SLA-Ti, SLA/5 × 10^{16}-Ag, SLA/1 × 10^{17}-Ag, SLA/5 × 10^{17}-Ag groups; 3D images of surface topography and roughness of SLA/5 × 10^{16}-Ag and

https://doi.org/10.1021/acsomega.3c04769
ACS Omega 2023, 8, 39269−39278

SLA/5 × 10^{17}-Ag groups; and water contact angle of SLA/5 × 10^{16}-Ag and SLA/5 × 10^{17}-Ag groups (PDF)

AUTHOR INFORMATION

Corresponding Authors

Dejun Li − *College of Physics and Materials Science, Tianjin Normal University, Tianjin 300387, China*; Email: dejunli@mail.tjnu.edu.cn

Sujuan Zeng − *Department of Pediatric dentistry, School and Hospital of Stomatology, Guangdong Engineering Research Center of Oral Restoration and Reconstruction, Guangzhou Key Laboratory of Basic and Applied Research of Oral Regenerative Medicine, Guangzhou Medical University, Guangzhou, Guangdong 510182, China*; Email: Zengsujuan78@foxmail.com

Authors

Ming Ma − *Department of Pediatric dentistry, School and Hospital of Stomatology, Guangdong Engineering Research Center of Oral Restoration and Reconstruction, Guangzhou Key Laboratory of Basic and Applied Research of Oral Regenerative Medicine, Guangzhou Medical University, Guangzhou, Guangdong 510182, China*

Mengli Zhao − *School of Electronic Engineering, Chaohu University, Anhui 238024, China*; orcid.org/0000-0003-2016-1621

Ruotong Ji − *Department of Pediatric dentistry, School and Hospital of Stomatology, Guangdong Engineering Research Center of Oral Restoration and Reconstruction, Guangzhou Key Laboratory of Basic and Applied Research of Oral Regenerative Medicine, Guangzhou Medical University, Guangzhou, Guangdong 510182, China*

Yi Guo − *Department of Pediatric dentistry, School and Hospital of Stomatology, Guangdong Engineering Research Center of Oral Restoration and Reconstruction, Guangzhou Key Laboratory of Basic and Applied Research of Oral Regenerative Medicine, Guangzhou Medical University, Guangzhou, Guangdong 510182, China*

Complete contact information is available at: https://pubs.acs.org/10.1021/acsomega.3c04769

Author Contributions

#M.M. and M.Z. contributed equally to this work. M.M.: Conceptualization, methodology, data curation, writing—original draft, writing—review and editing. M.l.Z.: Conceptualization, methodology, writing—review and editing. R.J.: Data curation, visualization, investigation. Y.G.: Data curation, visualization, investigation. D.L.: Conceptualization, methodology, writing—review and editing, supervision, funding acquisition. S.Z.: Conceptualization, methodology, writing—review and editing, supervision, funding acquisition.

Notes

The authors declare no competing financial interest.

ACKNOWLEDGMENTS

This research was financially supported by Guangzhou Health Science and Technology Project General Guidance Project (20231A011105); Guang Zhou Postdoctoral Research Start-up Funding (2022055287); and Guangzhou Medical University Research Ability Enhancement Project (02-410-2302184). The funders had no role in the study design and collection, analysis, and interpretation of the results.

ABBREVIATIONS

SEM,scanning electron microscopy; SLA,titanium surfaces treated by sandblasting with large grit and acid etching procedure; SLA/1 × 10^{17}-Ag,SLA-Ti were modified by TiN/Ag multilayers at Ag+ doses of 1× 10^{17} ions/cm^2; SLA/1 × 10^{18}-Ag,SLA-Ti were modified by TiN/Ag multilayers at Ag+ doses of 1× 10^{18} ions/cm^2; (*p < 0.05, **p < 0.01, ***p < 0.001)

REFERENCES

(1) Saruta, J.; Sato, N.; Ishijima, M.; Okubo, T.; Hirota, M.; Ogawa, T. Disproportionate Effect of Sub-Micron Topography on Osteoconductive Capability of Titanium. *Int. J. Mol. Sci.* **2019**, *20*, 4027.

(2) Shin, Y. C.; Bae, J. H.; Lee, J. H.; Raja, I. S.; Kang, M. S.; Kim, B.; et al. Enhanced Osseointegration of Dental Implants with Reduced Graphene Oxide Coating. *Biomater. Res.* **2022**, *26*, 11.

(3) Zhang, Y.; Chen, S. E.; Shao, J.; Beucken, J. V. D. Combinatorial Surface Roughness Effects on Osteoclastogenesis and Osteogenesis. *ACS Appl. Mater. Interfaces.* **2018**, *10*, 36652−36663.

(4) Wang, W. R.; Li, J.; Gu, J. T.; Hu, B. W.; Qin, W.; Zhu, Y. N.; et al. Optimization of Lactoferrin-Derived Amyloid Coating for Enhancing Soft Tissue Seal and Antibacterial Activity of Titanium Implants. *Adv. Healthc. Mater.* **2023**, *12*, No. e2203086.

(5) Wei, J.; Qiao, S.; Zhang, X.; Li, Y.; Zhang, Y.; Wei, S.; et al. Graphene-Reinforced Titanium Enhances Soft Tissue Seal. *Front Bioeng. Biotechnol.* **2021**, *9*, No. 665305.

(6) Yoon, S. W.; Kim, M. J.; Paeng, K. W.; Yu, K. A.; Lee, C. K.; Song, Y. W.; et al. Efficacy of Local Minocycline Agents in Treating Peri-Implantitis: An Experimental In Vivo Study in Beagle Dogs. *Pharmaceutics.* **2020**, *12*, 1016.

(7) Sun, H.; Chan, Y.; Li, X.; Xu, R.; Zhang, Z.; Hu, X.; et al. Multi-omics Analysis of Oral Bacterial Biofilm on Titanium Oxide Nanostructure Modified Implant Surface: In vivo Sequencing-based Pilot Study in Beagle Dogs. *Mater. Today Bio.* **2022**, *15*, No. 100275.

(8) Boyd, J. D.; Stromberg, A. J.; Miller, C. S.; Grady, M. E. Biofilm and Cell Adhesion Strength on Dental Implant Surfaces via the Laser Spallation Technique. *Dent. Mater.* **2021**, *37*, 48−59.

(9) Eger, M.; Hiram-bab, S.; Liron, T.; Sterer, N.; Carmi, Y.; Kohavi, D.; et al. Mechanism and Prevention of Titanium Particle-Induced Inflammation and Osteolysis. *Front Immunol.* **2018**, *9*, 2963.

(10) Ao, H.; Zong, J.; Nie, Y.; Wan, Y.; Zheng, X. An in vivo Study on the Effect of Coating Stability on Osteointegration Performance of Collagen/hyaluronic Acid Multilayer Modified Titanium Implants. *Bioact. Mater.* **2018**, *3*, 97−101.

(11) Sabino, R. M.; Mondini, G.; Kipper, M. J.; Martins, A. F.; Popat, K. C. Tanfloc/heparin Polyelectrolyte Multilayers Improve Osteogenic Differentiation of Adipose-derived Stem Cells on Titania Nanotube Surfaces. *Carbohydr. Polym.* **2021**, *251*, No. 117079.

(12) Awad, K.; Young, S.; Aswath, P.; Varanasi, V. Interfacial Adhesion and Surface Bioactivity of Anodized Titanium Modified with SiON and SiONP Surface Coatings. *Surf. Interfaces.* **2022**, *28*, No. 101645.

(13) Fu, J.; Zhu, W.; Liu, X.; Liang, C.; Zheng, Y.; Li, Z.; et al. Self-Activating Anti-infection Implant. *Nat. Commun.* **2021**, *12*, 6907.

(14) Shi, X.; Xu, L.; Munar, M. L.; Ishikawa, K. Hydrothermal Treatment for TiN as Abrasion Resistant Dental Implant Coating and Its Fibroblast Response. *Mater. Sci. Eng. C Mater. Biol. Appl.* **2015**, *49*, 1−6.

(15) Sun, X.; Gong, H.; Li, D.; Dong, L.; Zhao, M.; Wan, R.; et al. Ag^+ Implantation Induces Mechanical Properties, Cell Adhesion and Antibacterial Effects of TiN/Ag Multilayers in vitro. *Nanomedicine (Lond).* **2017**, *12*, 2257−2268.

(16) Kelly, P. J.; Li, H.; Whitehead, K. A.; Verran, J.; Arnell, R. D.; Iordanova, I. A Study of the Antimicrobial and Tribological Properties of TiN/Ag Nanocomposite Coatings. *Surf. Coat. Technol.* **2009**, *204*, 1137−1140.

(17) Zhao, M.; Gong, H.; Ma, M.; Dong, L.; Huang, M.; Wan, R.; et al. A Comparative Antibacterial Activity and Cytocompatibility for

Different Top Layers of TiN, Ag or TiN-Ag on Nanoscale TiN/Ag Multilayers. *Appl. Surf. Sci.* **2019**, *473*, 334−342.
(18) Singh, H.; Du, J.; Singh, P.; Yi, T. H. Extracellular Synthesis of Silver Nanoparticles by Pseudomonas Sp. THG-LS1.4 and Their Antimicrobial Application. *J. Pharm. Anal.* **2018**, *8*, 258−264.
(19) Villatte, G.; Massard, C.; Descamps, S.; Sibaud, Y.; Forestier, C.; Awitor, K. O. Photoactive TiO_2 Antibacterial Coating on Surgical External Fixation Pins for Clinical Application. *Int. J. Nanomedicine* **2015**, *10*, 3367−3375.
(20) Xue, Y.; Hong, X.; Gao, J.; Shen, R.; Ye, Z. Preparation and Biological Characterization of the Mixture of Poly(lactic-co-glycolic acid)/chitosan/Ag Nanoparticles for Periodontal Tissue Engineering. *Int. J. Nanomedicine* **2019**, *14*, 483−498.
(21) García, I.; Trobajo, C.; Amghouz, Z.; Alonso-guervos, M.; Díaz, R.; Mendoza, R.; et al. Ag- and Sr-enriched nanofibrous titanium phosphate phases as potential antimicrobial cement and coating for a biomedical alloy. *Mater. Sci. Eng., C* **2021**, *126*, No. 112168.
(22) Wang, H.; Yan, A.; Liu, Z.; Yang, X.; Xu, Z.; Wang, Y.; et al. Deciphering Molecular Mechanism of Silver by Integrated Omic Approaches Enables Enhancing Its Antimicrobial Efficacy in E. coli. *PLoS Biol.* **2019**, *17*, No. e3000292.
(23) Wang, Y. C.; Lin, S. H.; Chien, C. S.; Kung, J. C.; Shih, C. J. In Vitro Bioactivity and Antibacterial Effects of a Silver-Containing Mesoporous Bioactive Glass Film on the Surface of Titanium Implants. *Int. J. Mol. Sci.* **2022**, *23*, 9291.
(24) Shi, A.; Zhu, C.; Fu, S.; Wang, R.; Qin, G.; Chen, D.; et al. What Controls the Antibacterial Activity of Ti-Ag Alloy, Ag Ion or Ti(2)Ag Particles? *Mater. Sci. Eng., C* **2020**, *109*, No. 110548.
(25) Akhavan, O.; Ghaderi, E. Enhancement of antibacterial properties of Ag nanorods by electric field. *Sci. Technol. Adv. Mater.* **2009**, *10*, No. 015003.
(26) Wan, R.; Chu, S.; Wang, X.; Lei, L.; Tang, H.; Hu, G. Study on the Osteogenesis of Rat Mesenchymal Stem Cells and the Long-term Antibacterial Activity of Staphylococcus Epidermidis on the Surface of Silver-rich TiN/Ag Modified Titanium Alloy. *J. Biomed. Mater. Res., Part B.* **2020**, *108*, 3008−3021.
(27) Zhu, W. Q.; Shao, S. Y.; Xu, L. N.; Chen, W. Q.; Yu, X. Y.; Tang, K. M.; et al. Enhanced Corrosion Resistance of Zinc-containing Nanowires-modified Titanium Surface Under Exposure to Oxidizing Microenvironment. *J. Nanobiotechnology* **2019**, *17*, 55.
(28) Ma, M.; Zhao, M.; Deng, H.; Liu, Z.; Wang, L.; Ge, L. Facile and Versatile Strategy for Fabrication of Highly Bacteriostatic and Biocompatible SLA-Ti Surfaces with the Regulation of Mg/Cu Coimplantation Ratio for Dental Implant Applications. *Colloids Surf., B* **2023**, *223*, No. 113180.
(29) Sriubas, M.; Bockute, K.; Palevicius, P.; Kaminskas, M.; Rinkevicius, Z.; Ragulskis.; et al. Antibacterial Activity of Silver and Gold Particles Formed on Titania Thin Films. *Nanomaterials* **2022**, *12*, 1190.
(30) Lou, H. Y.; Zhao, W.; Li, X.; Duan, L.; Powers, A.; Akamatsu, M.; et al. Membrane Curvature Underlies Actin Reorganization in Response to Nanoscale Surface Topography. *Proc. Natl. Acad. Sci. U. S. A.* **2019**, *116*, 23143−23151.
(31) Xu, X.; Li, Y.; Wang, L.; Li, Y.; Pan, J.; Fu, X. Triple-functional Polyetheretherketone Surface with Enhanced Bacteriostasis and Anti-inflammatory and Osseointegrative Properties for Implant Application. *Biomaterials.* **2019**, *212*, 98−114.
(32) Ramakrishnaiah, R.; Alkheraif, A. A.; Divakar, D. D.; Matinlinna, J. P.; Vallittu, P. K. The Effect of Hydrofluoric Acid Etching Duration on the Surface Micromorphology, Roughness, and Wettability of Dental Ceramics. *Int. J. Mol. Sci.* **2016**, *17*, 822.
(33) Vlacic-zischke, J.; Hamlet, S. M.; Friis, T.; Tonetti, M. S.; Ivanovski, S. The Influence of Surface Microroughness and Hydrophilicity of Titanium on the Up-regulation of TGFβ/BMP Signalling in Osteoblasts. *Biomaterials* **2011**, *32*, 665−671.
(34) Cao, H.; Liu, X.; Meng, F.; Chu, P. K. Biological Actions of Silver Nanoparticles Embedded in Titanium Controlled by Micro-galvanic Effects. *Biomaterials* **2011**, *32*, 693−705.
(35) Chen, M.; Ouyang, L.; Lu, T.; Wang, H.; Meng, F.; Yang, Y.; et al. Enhanced Bioactivity and Bacteriostasis of Surface Fluorinated Polyetheretherketone. *ACS Appl. Mater. Interfaces* **2017**, *9*, 16824−16833.
(36) Li, W. R.; Xie, X. B.; Shi, Q. S.; Zeng, H. Y.; Ou-yang, Y. S.; Chen, Y. B. Antibacterial Activity and Mechanism of Silver Nanoparticles on Escherichia coli. *Appl. Microbiol. Biotechnol.* **2010**, *85*, 1115−1122.
(37) Shang, H.; Zhou, Z.; Wu, X.; Li, X.; Xu, Y. Sunlight-Induced Synthesis of Non-Target Biosafety Silver Nanoparticles for the Control of Rice Bacterial Diseases. *Nanomaterials* **2020**, *10*, 2007.
(38) Subbiah, R.; Jeon, S. B.; Park, K.; Ahn, S. J.; Yun, K. Investigation of Cellular Responses Upon Interaction with Silver Nanoparticles. *Int. J. Nanomedicine* **2015**, *10*, 191−201.
(39) Huang, Y. C.; Yang, T. Y.; Chen, B. X.; Kung, J. C.; Shih, C. J. Evaluation of Antibacterial Effects of Matrix-Induced Silver Ions against Antibiotic-Resistant ESKAPE Pathogens. *Pharmaceuticals* **2021**, *14*, 1094.
(40) Cao, H.; Qiao, Y.; Liu, X.; Lu, T.; Cui, T.; Meng, F. Electron Storage Mediated Dark Antibacterial Action of Bound Silver Nanoparticles: Smaller is Not Always Better. *Acta Biomater.* **2013**, *9*, 5100−5110.
(41) Zhu, Y.; Cao, H.; Qiao, S.; Wang, M.; Gu, Y.; Luo, H. Hierarchical Micro/nanostructured Titanium with Balanced Actions to Bacterial and Mammalian Cells for Dental Implants. *Int. J. Nanomedicine* **2015**, *10*, 6659−6674.
(42) Gittens, R. A.; Mclachlan, T.; Olivares-navarrete, R.; Cai, Y.; Berner, S.; Tannenbaum, R. The Effects of Combined Micron-/submicron-scale Surface Roughness and Nanoscale Features on Cell Proliferation and Differentiation. *Biomaterials* **2011**, *32*, 3395−3403.
(43) Olivares-navarrete, R.; Gittens, R. A.; Schneider, J. M.; Hyzy, S. L.; Haithcock, D. A.; Ullrich, P. F. Osteoblasts Exhibit a More Differentiated Phenotype and Increased Bone Morphogenetic Protein Production on Titanium Alloy Substrates than on Poly-ether-ether-ketone. *Spine J.* **2012**, *12*, 265−272.
(44) Sola-ruiz, M. F.; Perez-martinez, C.; Labaig-rueda, C.; Carda, C.; Martín de llano, J. J. Behavior of Human Osteoblast Cells Cultured on Titanium Discs in Relation to Surface Roughness and Presence of Melatonin. *Int. J. Mol. Sci.* **2017**, *18*, 823.
(45) Wu, S.; Xu, J.; Zou, L.; Luo, S.; Yao, R.; Zheng, B.; et al. Long-lasting Renewable Antibacterial Porous Polymeric Coatings Enable Titanium Biomaterials to Prevent and Treat Peri-implant Infection. *Nat. Commun.* **2021**, *12*, 3303.
(46) Zhou, W.; Peng, X.; Ma, Y.; Hu, Y.; Wu, Y.; Lan, F.; et al. Two-staged Time-dependent Materials for the Prevention of Implant-related Infections. *Acta Biomater.* **2020**, *101*, 128−140.
(47) Kim, J. C.; Lee, M.; Yeo, I. L. Three Interfaces of the Dental Implant System and Their Clinical Effects on Hard and Soft Tissues. *Mater. Horiz.* **2022**, *9*, 1387−1411.

https://doi.org/10.1021/acsomega.3c04769
ACS Omega 2023, 8, 39269−39278